Research Square

Preprints are preliminary reports that have not undergone peer review.
They should not be considered conclusive, used to inform clinical practice,
or referenced by the media as validated information.

CGRP–TGF-β/Smad2/3 Axis Mediates the Translation of Sensory Neuropeptide Signals into BMSCs Osteogenic Differentiation and Promotes Bone Regeneration

Xi Wang
First Affiliated Hospital of Xinjiang Medical University
Qiyu Jia
Nankai University
Maihemuti Yakufu
Sixth Affiliated Hospital of Xinjiang Medical University
Junru Liao
First Affiliated Hospital of Xinjiang Medical University
Jun Zhang
First Affiliated Hospital of Xinjiang Medical University
Meng Zhao
First Affiliated Hospital of Xinjiang Medical University
Jinyong Huang
First Affiliated Hospital of Xinjiang Medical University
Jingcheng Hu
First Affiliated Hospital of Xinjiang Medical University
Yanbin Zhu
Third Hospital of Hebei Medical University
Chuang Ma
MaChuang@xjmu.edu.cn

First Affiliated Hospital of Xinjiang Medical University

Research Article

Keywords: CGRP, TGF-β/Smad, bone regeneration

Posted Date: November 23rd, 2026

DOI: https://doi.org/10.21203/rs.3.rs-11285776/v1

License: This work is licensed under a Creative Commons Attribution 4.0 International License.
Read Full License

Additional Declarations: No competing interests reported.

CGRP–TGF-β/Smad2/3 Axis Mediates the Translation of Sensory Neuropeptide Signals into BMSCs Osteogenic Differentiation and Promotes Bone Regeneration

Xi Wang[a†], Qiyu Jia[b†], Maihemuti Yakufu[c†], Junru Liao[a], Jun Zhang[a], Meng Zhao[a], Jinyong Huang[a], Jingcheng Hu[a], Yanbin Zhu[d,e,f,g*], Chuang Ma[a*]

[a] Department of Trauma Orthopedics, The First Affiliated Hospital of Xinjiang Medical University, Urumqi, 830000, China

[b] School of Medicine, Nankai University, Tianjin 300071, China

[c] Department of Sports Medicine, Sixth Affiliated Hospital of Xinjiang Medical University, Tianshan District, Urumqi 830002, PR China

[d] Department of Orthopaedic Surgery, Hebei Medical University Third Hospital, Shijiazhuang, Hebei, 050000, China

[e] Key Laboratory of Biomechanics of Hebei Province, Shijiazhuang, Hebei, China;

[f] NHC Key Laboratory of Intelligent Orthopaedic Equipment, Shijiazhuang, Hebei, China;

[g] Engineering Research Center of Orthopedic MinimallyInvasive Intelligent Equipment, Ministry of Education, Shijiazhuang, Hebei, China

[*] **Corresponding authors.**

E-mail: 38600312@hebmu.edu.cn (Yanbin Zhu) and E-mail: machuang@xjmu.edu.cn (Chuang Ma)

[†] **Xi Wang, Qiyu Jia and Maihemuti Yakufu contributed equally to this work.**

Abstract：

Sensory nerves do more than register skeletal injury; they actively direct repair, with calcitonin gene-related peptide (CGRP) serving as a principal messenger. However, how bone marrow mesenchymal stem cells (BMSCs) decode this cue remains poorly defined, and rapid clearance severely limits CGRP's translational utility.

Unbiased RNA sequencing of CGRP-treated rat BMSCs revealed a selective response of 275 differentially expressed genes, prominently enriched in TGF-β signaling. CGRP promoted BMSC proliferative activity, migration, alkaline phosphatase activity, and mineralization. Mechanistically, CGRP induced Smad2/3 phosphorylation and nuclear translocation without altering total Smad2/3 abundance. Blocking either node independently, the CGRP receptor with rimegepant or ALK4/5/7

with SB-431542, was sufficient to suppress the CGRP-driven osteogenic response, placing the TGF-β/Smad2/3 cascade in the causal path rather than alongside it.

To overcome clearance in vivo, CGRP was loaded into a photocurable HAMA/GelDA hydrogel that released the peptide biphasically, an initial burst followed by sustained release beyond two weeks, a profile timed against the reported course of CGRP-positive fiber ingrowth in the callus. In a rat skull defect model, compared with the use of hydrogel alone, CGRP-releasing hydrogel promoted new bone formation at the cranial defect site at weeks 4 and 8, accompanied by increased local levels of TGF-β, Smad2/3, OCN, and BMP4.

Collectively, these findings define a receptor-dependent CGRP–TGF-β/Smad2/3 axis in BMSCs and identify Smad2/3 activation as the intracellular step through which a sensory neuropeptide signal is converted into osteogenic commitment, providing a mechanistic entry point into the neuro-osseous axis.

Keywords: CGRP; TGF-β/Smad; bone regeneration;

1. Introduction

The restoration of extensive segmental bone defects poses a significant clinical challenge. Traditional bone tissue engineering paradigms have primarily focused on achieving recovery of mechanical properties and macroscopic structure by actively interacting with local cells, such as osteoblasts, to initiate bone healing responses[1,2]. However, a growing body of evidence suggests that efficient bone regeneration is not an isolated event mediated by a particular cell type or a particular material, but rather depends on the coordinated remodeling of the neural, vascular, immune, and osteogenic microenvironments[3-5]. Peripheral sensory neurons, which are distributed extensively throughout the periosteum and bone marrow, are increasingly being redefined from mere anatomical features to active regulators of bone homeostasis[6,7].

In the initial stages of bone injury, sensory nerve endings undergo extensive extension and regeneration within the bone callus; these fibers release various neuropeptides to remodel the local microenvironment[8,9]. Sensory neurons modulate the bone microenvironment by releasing neuropeptides, neurotrophic factors, and bioactive substances[10,11]. For example, nerve growth factor (NGF) is highly expressed after fracture; through activation of its receptor tropomyosin receptor kinase A (TrkA), it can repair injured sensory nerves and also promote osteogenesis[12]. Therefore, sensory nerves play a crucial role in the regulation of bone metabolism, and elucidating how BMSCs perceive sensory nerve signals and translate them into osteogenic signals is a key scientific challenge in deciphering the mechanism of the “neuro-osseous axis.”

CGRP is the core neuropeptide released by sensory neurons[13]. Both clinical and basic research have reported significant enrichment of CGRP-positive nerve fibers in fracture healing areas. Inhibiting sensory nerve signaling impedes the formation of the vascular-nervous network at the fracture site, thereby delays the mineralization of the callus[8,14]. However, an unresolved biological question remains: neuropeptide signals such as CGRP are typically characterized by short duration and rapid metabolism, whereas bone regeneration is a tissue reconstruction process that lasts for weeks or even longer. In other words, how transient neuropeptide stimulation is converted by BMSCs into a relatively sustained osteogenic differentiation program still lacks systematic elucidation.

To identify this potential transducing node without presupposing a single pathway, we performed RNA-seq on BMSCs treated with CGRP to comprehensively track molecular trajectories.

Unbiased transcriptomic analysis revealed that CGRP not only indirectly regulates voltage-gated calcium channels through intracellular signaling cascades, promoting extracellular calcium influx and triggering physiological activities such as neurotransmitter release, muscle contraction, and hormone secretion, but also enhances chemokine receptor binding on the cell surface, activates intracellular signaling, and promotes cell proliferation, adhesion, and migration. More importantly, the transcriptomic data clearly pointed to the significant enrichment and response of the TGF-β signaling pathway following CGRP intervention.

As one of the core signals regulating the osteogenic differentiation fate of MSCs during bone regeneration, TGF-β not only acts as a chemokine to recruit MSCs to the site of injury but also precisely regulates their osteogenic differentiation fate by initiating various signaling events, including differentiation, apoptosis, and migration[15,16]. Mechanistically, TGF-β induces Runx2 expression through a Smad-dependent signaling cascade, which in turn initiates the osteogenic differentiation program in MSCs[17,18]. In view of this, we hypothesize that the TGF-β/Smad signaling axis may act as an important transducing bridge that links upstream transient neuropeptide stimulation to downstream sustained osteogenic effects in BMSCs.

However, validation of the above mechanism faces a practical challenge: CGRP, as a polypeptide lacking quaternary protein structure[19], has a short half-life and is rapidly metabolized, leading to quick degradation in plasma and an inability to maintain effective concentrations required for initiating osteogenic programs in bone defect areas[20]. To overcome this half-life barrier and to enable real-time mechanistic observation in situ, we introduced a photocurable hydrogel as a local sustained-release carrier[21,22]. This carrier was designed to biomimetically simulate the release of sensory neuropeptides in the bone defect region, thereby providing the necessary spatiotemporal support for validating the osteogenic effects of the TGF-β/Smad2/3 signaling axis in a rat calvarial defect model.

Based on this, we constructed a continuous chain of evidence encompassing in vitro transcriptomic screening, targeted signaling pathway inhibition, in vivo biomimetic delivery, and bone regeneration evaluation. This study not only systematically elucidates, at the molecular level, the potential mechanism by which CGRP induces TGF-β/Smad2/3 signaling axis activation and drives BMSC osteogenesis, but also provides evidence for understanding how transient neural signals are translated into sustained osteogenic programs, offering new theoretical support for repair

strategies targeting the neuro-bone axis.

2. Materials and Methods

2.1 Isolation of BMSCs

All animal experimentation procedures were approved by the Institutional Animal Care and Use Committee (IACUC) of Xinjiang Medical University (Approval No.: IACUCJT 2026011501). Primary BMSCs were isolated from 3-4-week-old male Sprague-Dawley rats (weighing approximately 40-80g). In accordance with the IACUC-approved protocol, the rats were euthanized by cervical dislocation following deep anesthesia with isoflurane. Under aseptic conditions, the femur and tibia were dissected; the epiphyses were trimmed to expose the medullary cavity, which was then flushed with α-MEM containing 1% penicillin-streptomycin. The collected cell suspension was centrifuged at 1000 rpm for 5 min; the supernatant was discarded, and the cell pellet was resuspended in complete medium (α-MEM containing 10% fetal bovine serum and 1% penicillin-streptomycin; Gibco, USA; Biosharp, China) and then inoculated into culture. The cells were used for subsequent experiments after being passaged to the third generation. In this study, "n=3" for BMSC-related experiments refers to three independent technical replicates performed on the same batch of third-generation BMSCs under the same experimental conditions.

2.2 Experimental group division

To systematically analyze the biological functions of CGRP and its downstream mechanisms, this study designed two independent cellular intervention experiments. Experiment 1 aimed to validate the osteogenic effects of CGRP and included a blank control group, a group treated with CGRP alone, and a group treated with CGRP in combination with a CGRP receptor antagonist. Experiment 2 was designed to determine whether the TGF-β is a primary downstream component of CGRP-mediated osteogenesis. This experiment included a TGF-β inhibitor group, a group treated with CGRP alone, and a group treated with a combination of CGRP and a TGF-β inhibitor. The TGF-β inhibitor (SB-431542, MCE) at a concentration of 3×10^{-6} mol/L effectively inhibits the function of TGF-β receptors in BMSCs and effectively blocks the function of tissue signaling targets[23]. Therefore, we chose this concentration as the cell intervention concentration. Rimegepant (CGRP receptor antagonists, HY-15498, MCE) has no cytotoxicity at concentrations below 1×10^{-6} mol/L[24].

2.3 Flow Cytometric Identification

For immunophenotyping, approximately 1×10^{6} BMSCs per aliquot were stained with fluorescence-

conjugated antibodies against CD90-FITC, CD45-FITC, CD11b/c-FITC(Biolegend), and CD29-PE (BD Biosciences), with an unstained control for autofluorescence. After washing with PBS, the cells were resuspended in pre-chilled PBS and filtered through a 200-mesh nylon mesh to obtain a uniform cell suspension. Subsequently, flow cytometry data were collected using a Beckman Coulter flow cytometer.

2.4 CCK-8

Following the grouping scheme described in Section 2.2, "Experiment 1," cultured cells were treated with the drug at different concentration gradients. On days 1, 2, and 3, the CCK-8 assay was used to evaluate cell proliferation. The samples were incubated at 37°C for 1 hour, after which the absorbance values were measured. The OD values for OD3 (experimental group), OD2 (control group), and OD1 (background group) were recorded separately.

$$\text{Cell Activities}(\%) = \frac{OD3-OD1}{OD2-OD1}\times 100\%$$

2.5 Transwell

Starve the cells for 24 hours, then seed 1×10^5 cells into serum-free transwell chambers; add complete medium containing the corresponding drug (as described in the experimental grouping scheme in Section 2.2) to the lower chamber. After 24 hours, remove the transwell chamber and fix the cells with paraformaldehyde for 30 minutes. Next, the filter membrane chamber was stained for 30 minutes using a 0.1% crystal violet solution. Randomly select fields of view under a microscope and take photographs; analysis was performed using ImageJ software.

2.6 Alkaline phosphatase (ALP) staining

Seed the cells in a 6-well plate and induce osteogenic differentiation for 7 days. After fixing the cells with 4% paraformaldehyde, perform ALP staining according to the instructions for the BCIP/NBT ALP Staining Kit (Beyotime). Take photographs under a microscope and perform quantitative analysis using ImageJ software.

2.7 Alizarin red S (ARS) staining for mineralized nodule assessment

Using the same method as in the ALP staining experiment, cells were seeded in 3.5-cm culture dishes (previously coated with 0.1% gelatin) and underwent osteogenic induction for 25 days. After fixation with 4% paraformaldehyde, the samples were stained with alizarin red S (Amizona, China) for 30 minutes, followed by gentle rinsing with distilled water. Photographs were taken under a

microscope, and quantitative analysis was performed using ImageJ software.

2.8 Transcriptome analysis and functional enrichment

For RNA-seq, three technical replicate libraries were prepared from the same batch of passage-3 BMSCs under identical conditions for each group (the control group and the CGRP group), and all libraries were sequenced (n=3 per group). A library was constructed using 1 μg of total RNA. Poly(A) mRNA was enriched using Oligo(dT) magnetic beads, and the first strand cDNA was synthesized using random primers. The library was then prepared using the VAHTS® Universal V8 RNA-seq Library Prep Kit for Illumina (Vazyme) and sequenced on the Illumina platform in a 2×150 bp paired-end mode. The original reads were trimmed using Cutadapt (v1.9.1), with the removal of adapters and low-quality bases (Phred score < 20, maximum error rate 0.1, minimum length 75 bp, maximum N ratio 0.1), and quality checks were performed using FastQC (v0.11.9). The clean reads were aligned to the Rattus norvegicus Rnor_6.0 reference genome using HISAT2 (v2.2.1). Gene-level counts were generated using HTSeq (v0.6.1) based on Ensembl Rnor_6.0 (release 104) in a strand-specific mode.

Differential expression analysis was performed using DESeq2 (version 1.34.0) based on a negative binomial distribution model, with normalization using the median ratio method, followed by Wald tests and Benjamini–Hochberg correction. Genes satisfying $|\log_2 FC| \geq 1$ and FDR < 0.05 were defined as differentially expressed genes (DEGs). GSEA was performed on the MSigDB Hallmark, GO, and KEGG gene sets using gseapy (version 0.9.5), with genes ranked based on $\log_2 FC$; an FDR < 0.25 was considered statistically significant. Using all expressed genes as the background, GO enrichment analysis of DEGs was performed using GOSeq (version 1.34.1), which corrects for gene length bias, while KEGG enrichment analysis was performed using the hypergeometric test. An FDR < 0.05 was considered statistically significant.

2.9 Alternative splicing (AS) analysis

In order to evaluate the transcriptome diversity and differential regulation between conditions, based on the BAM file generated by HISAT2 alignment, rMATS (v4.1.0) was used to analyze the differential AS events between the control group and the CGRP group. Five major splicing types were evaluated, including exon skipping (SE), alternative 5' splice site (A5SS), alternative 3' splice site (A3SS), mutually exclusive exon (MXE) and intron retention (RI). The threshold of | IncLevelDifference | ≥ 0.1 and FDR < 0.05 was used to identify and report statistically significant

differential splicing events.

2.10 qRT-PCR

The mRNA levels of osteogenic markers in CGRP-treated BMSCs were determined by qRT-PCR. RNA extraction (Foregene, China) and cDNA synthesis (Servicebio, China) were supplied protocols. Relative expression levels were normalized to GAPDH and computed using the $2^{-\Delta\Delta Ct}$ method, with each group tested in triplicate (primer details in Table 1).

2.11 Western blot

Cells were lysed using RIPA lysis buffer (Solarbio, China) and protein quantification was performed using the BCA method (Thermo, USA). After electrophoresis on SDS-PAGE (Biotides, China) and membrane transfer, the membranes were blocked, followed by overnight incubation with the primary antibody at 4°C. The membranes were then incubated for 1 hour with HRP-labeled anti-rabbit secondary antibody (1:5000). Development and imaging were performed using ECL (Biosharp, China). Density was measured using ImageJ 1.46 r, with GAPDH serving as the internal control. The primary antibodies (ALP, RUNX2, TGF-β, TGF-βR, BMP4, Smad2/3, p-Smad2/3) were diluted at a ratio of 1:1000, and GAPDH was diluted at a ratio of 1:5000.

2.12 Immunofluorescence

After 7 days of osteogenic induction, the BMSCs were fixed (4% PFA, 30 minutes), permeabilized (0.3% Triton X-100), and blocked (3% BSA). TGF-β and Smad2/3 were detected by incubating with the primary antibody (1:200) overnight at 4 °C, followed by a 60-minute incubation with the fluorescent secondary antibody (1:500). Nuclei were stained with DAPI, and images were acquired using a fluorescence microscope (ZEISS, Germany).

2.13 Animal surgery

A total of 12 male SD rats (10 weeks old, 300–350g) were used in this study. All animal experiments strictly adhered to the ARRIVE 2.0 guidelines and were approved by the Institutional Animal Care and Use Committee (IACUC) (Approval No.: IACUCJT 2026011501). Male rats were selected to avoid the interfering effects of estrogen on bone metabolism.

The experimental rats were randomly assigned to two groups (H2G5 group and H2G5@CGRP group) using a random number table. Prior to surgery, the rats were anesthetized via intraperitoneal injection of 3% sodium pentobarbital (0.2mL/100g). After routine disinfection, a 2-cm midline incision was made in the scalp. A standard 8-mm-diameter full-thickness cranial defect was created

in the frontal bone of each rat using a drill. The hydrogel was implanted into the defect site and photopolymerized in situ using 405-nm light. Subsequently, the periosteum and skin were sutured layer by layer. Postoperatively, the rats were housed individually and received routine injections of penicillin for 3 consecutive days to prevent infection. The surgeon was blinded to the group assignments during the procedure. Three rats were euthanized from each group at the 4-week and 8-week time points (three per group at each time point). This sample size was determined based on previous similar literature and the 3Rs principles (replacement, reduction, and refinement), with the aim of minimizing animal use while ensuring statistical reliability[26]. At the specified endpoints, the experimental rats were euthanized by an overdose of sodium pentobarbital injection. Death was confirmed prior to euthanasia by verifying the cessation of breathing and the absence of a cardiac reflex. Subsequently, the skulls and organs were collected for subsequent micro-CT scanning and histological staining. The researchers conducting the subsequent micro-CT scanning, histological evaluation, and data analysis were blinded to the group assignments.

2.14 Preparation of hydrogel

The hydrogel precursor was prepared following the procedures described in previously published articles[21,22]. In brief, the final precursor solution used in this study was prepared by dissolving HAMA, GelDA, and 0.2% (w/v) LAP photoinitiator in neutral PBS (pH=7.4) (H2G5). Furthermore, CGRP was added directly to the aforementioned precursor solution to prepare the drug-loaded hydrogel (H2G5@CGRP), with a final concentration of 40 μg/mL[27].

2.15 Micro-CT

With six rats per group allocated to two time-point subgroups (n=3 at 4 weeks and n=3 at 8 weeks), specimens were collected at the designated endpoints. Following 48h fixation in 4% paraformaldehyde, skulls were scanned using a micro-CT system (NMC-200, Pingsheng Science) under conditions of 80 kV, 0.06 mA, and 35 μm resolution. Recon software reconstructed the raw data in 3D, while Avatar software performed quantitative analysis. The ROI was set at the original defect borders, and bone volume fraction (BV/TV), trabecular bone thickness (Tb.Th), and trabecular bone number (Tb.N) were computed automatically. Data were exported to Excel. After CT imaging, all samples were processed for H&E, Masson, and IHC staining

2.16 Histological staining

Biosafety evaluation of the hydrogel in vivo was conducted using H&E staining on harvested organs

(heart, liver, spleen, lung, and kidney) from rats in each group. Tissue processing included paraformaldehyde fixation, paraffin embedding, sectioning, and H&E staining. Histopathological changes were observed microscopically for signs of toxicity such as inflammation and necrosis. Following micro-CT scanning, cranial specimens were subjected to decalcification with EDTA (Solarbio, China), graded alcohol dehydration, paraffin embedding, sectioning, and subsequent H&E (ServiceBio, China) and Masson staining.

2.17 Immunohistochemical (IHC) staining

Tissue sections were incubated with primary antibodies against OCN (1:100), BMP4 (1:100), TGF-β (1:200), and Smad2/3 (1:100), then incubated with secondary antibodies (1:500). Finally, the tissue sections were stained using DAB substrate (Servicebio, China), and the expression of osteogenic markers was visually assessed under a microscope (Nikon, Japan). All immunohistochemical sections were stained in the same batch, and the DAB development time was strictly standardized. The percentage of positive staining area for each marker was analyzed using digital slide viewing software (Servicebio, China).

2.18 Statistical analysis

Data are shown as mean ± SD. One-way ANOVA with Tukey's test was used for multiple in vitro group comparisons. In vivo data were analyzed by two-way ANOVA (treatment×time), with Šídák's adjustment for simple effects when interaction was significant, otherwise only main effects were reported. All tests were two-sided, $\alpha = 0.05$, using GraphPad Prism 9.5.0.

3. Results

3.1 CGRP-mediated in vitro osteogenic effects of BMSCs

To gain a deeper understanding of the osteogenic effects of CGRP on BMSCs, we isolated BMSCs from SD rats. Flow cytometry analysis of surface markers revealed high expression of CD29 (86.6%) and CD90 (94.7%), and low expression of CD45 (8.63%) and CD11b (0.46%) (Fig. 1A). The cell purity met the requirements for subsequent experiments.

The results of the CCK-8 assay reveal that, compared to the blank control group, CGRP promoted BMSC proliferation at all tested concentrations (1×10^{-6} to 1×10^{-9} mol/L) from days 1 to 3, with the most significant proliferative effect observed at a concentration of 1×10^{-7} mol/L. Therefore, 1×10^{-7} mol/L was selected as the optimal concentration for subsequent interventions. To confirm the specificity of CGRP-mediated cell proliferation, the CGRP receptor antagonist

(rimegepant) was administered at concentrations of 1×10^{-10}， 1×10^{-9}, 1×10^{-8}, and 1×10^{-7} mol/L in combination with a fixed dose of CGRP (1×10^{-7} mol/L). Antagonist concentrations of 1×10^{-8} and 1×10^{-7} mol/L effectively blocked CGRP-induced BMSCs proliferation, whereas concentrations of 1×10^{-10} and 1×10^{-9} mol/L were only partially effective. Based on study results showing that rimegepant exhibits no cytotoxicity at concentrations below 1×10^{-6} mol/L[24], 1×10^{-8} mol/L was selected as the working concentration for subsequent studies.

ALP staining results indicate that, when compared to the blank group, the CGRP group exhibited deeper and more extensive ALP-positive staining. After the addition of a CGRP receptor antagonist, ALP-positive staining became lighter (Fig. 1C, F, $P<0.05$). ARS staining results indicated that, when compared with the blank group, the CGRP group exhibited a greater number of calcium nodules with a broader distribution, whereas calcium nodule formation was significantly reduced in the CGRP receptor antagonist group (Fig. 1D, G, $P<0.05$). Transwell results revealed that the number of migrating cells in the CGRP-treated group was markedly higher than the blank group, while the CGRP receptor antagonist group exhibited the lowest number of migrating cells (Fig. 1E, H, $P<0.05$).

These results demonstrate that CGRP significantly enhances the proliferation, migration, and osteogenic differentiation of BMSCs, whereas antagonizing CGRP receptors inhibits these biological processes, indicating that CGRP plays a pivotal role in mediating the osteogenic differentiation of BMSCs.

3.2 CGRP can modulate the gene regulatory network of BMSCs in various biological functions

To further decode the translational mechanism by which CGRP regulates BMSCs fate within the "neuro-bone axis," we collected cell samples from the blank group and the CGRP-treated BMSCs group for transcriptomic analysis. RNA-Seq quality assessment confirmed high inter-sample consistency (Fig. S1)

Hierarchical cluster analysis revealed that the gene expression profile of BMSCs underwent significant changes following CGRP intervention (Figure 2A). Based on the results of the Volcano plot analysis, this study has identified a total of 275 DEGs, comprising 144 upregulated and 131 downregulated genes, while 19,353 genes did not meet the threshold for statistical significance (Figure 2B, Table S1). This result suggests that CGRP does not induce widespread and indiscriminate transcriptional alterations in BMSCs, but rather modulates their functional state

through a relatively focused molecular network.

GO analysis indicates that, following CGRP intervention, BMSCs exhibited significant gene enrichment across three functional categories. In terms of biological process (BP), enriched terms included cell adhesion and migration, regulation of cell proliferation, and inflammation and immune responses (Fig. 2C), indicating that CGRP may regulate BMSC growth and proliferation while also modulating local inflammatory status and immune responses. Furthermore, in the cellular component (CC) category, CGRP intervention led to enrichment of genes associated with multiple extracellular matrix (ECM)-related components and ECM assembly processes, suggesting that CGRP treatment significantly influences ECM composition and remodeling, thereby altering the cellular microenvironment. At the molecular functional (MF) level, GO enrichment analysis further identified several terms closely associated with osteogenic activity, notably calcium ion binding，protein homodimerization activity, heparin binding, growth factor activity, suggesting that CGRP may promote bone regeneration through these molecular mechanisms. In summary, CGRP regulates BMSCs cellular functions, the microenvironment, and molecular interaction networks in multiple dimensions through transcriptional reprogramming, thereby triggering cascade effects and promoting bone regeneration.

KEGG analysis indicates that these DEGs are extensively involved in three major functional domains: (1) metabolism-related pathways, including branched-chain amino acid synthesis and coenzyme A synthesis; (2) signaling pathways related to osteogenic differentiation, such as the TGF-β pathway and cytokine-cytokine receptor interactions; (3) pathways related to endocrine regulation, involving renin secretion, gonadotropin-releasing hormone (GnRH) secretion, and the biosynthesis of steroid hormones (Fig. 2D). Extensive evidence indicates that the TGF-β pathway has a decisive impact on embryonic development and the maintenance of homeostasis in the skeletal system after birth, primarily involving chondrocytes, osteoblasts, osteocytes, and osteoclasts[17]. KEGG enrichment analysis identified the TGF-β pathway, itself a key pathway in bone growth and development, suggesting that CGRP may mediate “neuro-osseous axis” signaling through the TGF-β pathway, thereby regulating bone regeneration.

Alternative splicing (AS) is an integral post-transcriptional regulatory mechanism in eukaryotes, typically mediated by the spliceosome recognizing and excising specific sequences from precursor mRNA, and represents an important process for modulating gene expression and

generating proteomic diversity[28]. To ensure the robustness of the AS results, we employed two analysis modes: Junction Counts (JC) and Junctions and Exons Combined Counting (JCEC). AS analysis revealed that CGRP treatment significantly reshaped the splicing landscape, predominantly affecting skipped exon and alternative 3′ splice site events (Fig. 2E, F, Table S2-S11).

GSEA analysis revealed that CGRP enhanced chromosome segregation and DNA replication processes in BMSCs (Fig. 2G). Cell proliferation requires precise distribution of replicated chromosomes into two daughter cells through mitosis, with chromosome segregation being the central step in this process[29]. DNA replication, as the core event of the S phase of the cell cycle, most directly reflects accelerated cell cycle progression[30]. Therefore, the GSEA enrichment of chromosome segregation and DNA replication processes suggests that the cells are actively undergoing division and proliferation, indicating that the neuropeptide CGRP mediates BMSCs cell cycle progression, thereby anchoring BMSCs cell fate.

Collectively, CGRP, as a key effector molecule of sensory neural signals, can be sensed by BMSCs and translated into multilayered transcriptomic reprogramming, encompassing gene expression, signaling pathway activation, alternative splicing regulation, and functional phenotypic output, ultimately translating neural microenvironment signals into precise biological instructions that promote BMSCs osteogenic differentiation. Among these, TGF-β signaling may be a key downstream component of this “neuro-osseous axis” signaling network.

3.3 CGRP activates the TGF-β/Smad2/3 signaling pathway to stimulate osteoblast differentiation

Based on the results of the KEGG analysis, we next investigated the contribution of the TGF-β signaling cascade to CGRP-induced osteogenic differentiation of BMSCs. Immunofluorescence staining results revealed that, when compared with the blank group, TGF-β immunoreactivity was significantly stronger following CGRP intervention, whereas the fluorescence signal in the CGRP receptor antagonist group was relatively weaker (Figure 3A). For Smad2/3, a predominantly cytoplasmic distribution was observed in the blank and CGRP receptor antagonist groups. In contrast, upon CGRP stimulation, Smad2/3 fluorescence was visibly enriched in the nuclear compartment, suggestive of nuclear translocation (Fig. 3B).

Additionally, in the initial transcriptomic screening, we observed significant up-regulation of BMP4, a member of the BMP family. Therefore, we designed and synthesized BMP4-specific

primers to investigate whether CGRP intervention promotes BMP4 expression. PCR results indicate that mRNA expression of osteogenesis-related genes (ALP, Runx2, OCN, and Bmp4) notably increased following CGRP treatment, whereas the addition of a CGRP receptor antagonist significantly suppressed the expression of these genes (Fig. 3C, $P<0.05$).

The mechanistic contribution of TGF-β signaling to the CGRP-mediated 'neuro-bone axis' was investigated by measuring protein expression levels of TGF-β, TGF-βR, Smad2/3, p-Smad2/3, and osteogenic markers (ALP, RUNX2, BMP4). Significant upregulation of TGF-β, TGF-βR, ALP, RUNX2, and BMP4 was detected in the CGRP group relative to the blank group, accompanied by an increased p-Smad2/3/total Smad2/3 ratio with unaltered total Smad2/3 levels. These CGRP-induced elevations were notably reversed upon treatment with the receptor antagonist (Fig. 3D, E, $P<0.05$). These results indicate that CGRP initiates downstream osteogenic signaling cascades predominantly through activating Smad2/3 phosphorylation, rather than altering its total protein expression.

The above results indicate that CGRP may activate TGF-βR-mediated Smad2/3 phosphorylation by upregulating the expression of TGF-β and its receptors, and that this increase in phosphorylation levels is accompanied by increased expression of osteogenesis-related genes, such as Runx2 and BMP4.

3.4 Inhibition of TGF-β attenuates BMSCs osteogenic differentiation mediated by CGRP

Furthermore, we used TGF-β inhibitors to confirm the critical role of the TGF-β pathway in the CGRP-mediated osteogenic differentiation of BMSCs. Transwell results demonstrated that the CGRP group exhibited the strongest cell migration capacity; however, upon the addition of a TGF-β inhibitor, the CGRP-mediated cell migration effect was significantly attenuated, indicating that blocking TGF-β can reduce CGRP-induced cell migration (Fig. 4A, B, $P<0.05$). ALP staining results demonstrated that the CGRP group displayed deeper staining and broader positive areas, while TGF-β inhibitor intervention attenuated the early osteogenic differentiation capacity induced by CGRP (Fig. 4E, C, $P<0.05$). ARS staining revealed that the CGRP group exhibited robust osteogenic mineralization, whereas TGF-β inhibitor treatment significantly reduced calcium nodule formation (Fig. 4F, D, $P<0.05$). CGRP-induced osteogenic differentiation of BMSCs depends, at least in part, on TGF-β signaling, as demonstrated by the functional assays described above.

To further investigate how CGRP-regulated TGF-β signaling affects the expression of

osteogenic factors during differentiation, we measured protein and mRNA levels following treatment with a TGF-β inhibitor. Western blot and qRT-PCR results showed that, in the presence of CGRP, the addition of a TGF-β inhibitor significantly reduced the protein levels of TGF-β, TGF-βR, and p-Smad2/3 mediated by CGRP (Fig. 4G, H, $P<0.05$)., and a similar trend was observed at the mRNA level (Fig. 4I, $P<0.05$).

Previous studies have established that TGF-β family members play indispensable roles in skeletal development and homeostasis[17]. Activation of the classic TGF-β signaling pathway begins with the phosphorylation of Smad2/3, which then forms a transcriptionally active complex with Smad4 and translocates into the cell nucleus. This complex recruits the osteogenesis-specific transcription factor RUNX2 to the promoter regions of target genes, thereby synergistically activating the transcription and protein expression of genes associated with osteogenic differentiation[31].

Taken together, the results indicate the TGF-β/Smad2/3 signaling axis is a key component of the CGRP-mediated osteogenic response in BMSCs. Although the current data do not definitively establish TGF-β/Smad2/3 as the sole pathway mediating CGRP action, the inhibition experiments support its role as a key downstream mechanism underlying CGRP-induced osteogenic responses in BMSCs.

3.5 In vivo delivery of CGRP promotes in situ bone regeneration, accompanied by activation of the TGF-β/Smad2/3 signaling pathway

As a critically important mediator in “neuro-osseous axis” interactions, CGRP is primarily cleared from the body by various proteases, resulting in extremely low bioavailability[13]. Given that CGRP is a polypeptide lacking quaternary structure, its plasma half-life is only approximately 7 minutes[32]. To address this limitation, we employed our previously developed ultra-adhesive H2G5 hydrogel as a localized sustained-release carrier to encapsulate CGRP, aiming to compensate for the bioavailability deficit imposed by its short half-life and to achieve stable, continuous release of CGRP within the bone defect area, thereby providing a sustained material basis for the downstream TGF-β/Smad2/3 signaling pathway[22,33].

To evaluated the biomimetic controlled-release properties of the CGRP@H2G5 hydrogel, we used the ELISA method to monitor its cumulative release behavior (Figure S2). The results displayed a biphasic release kinetics—a rapid release of a large amount of CGRP in the early phase

(7 days), subsequently transitioning to a steady, sustained release that lasted for at least 14 days. Previous histological observations in rat fracture models demonstrated that $CGRP^+$ sensory nerve fibers accounted for 83.0% of the total nerve population in the callus microenvironment at the early healing stage (day 3), and remained at a high level of 87.5% at the mid-healing stage (day 14), suggesting both an early acute initiation demand and a mid-to-late sustained supply requirement for CGRP during bone repair and regeneration[11]. The initial burst release from our material effectively mimics the transient massive release of local neuropeptides following injury, thereby rapidly initiating the cascade of bone regeneration; meanwhile, the subsequent sustained-release phase precisely aligns with the long-term physiological demand corresponding to the persistently high proportion of $CGRP^+$ fibers within the callus. Thus, this biphasic sequential release mode adequately recapitulates, in vitro, the spatiotemporal supply dynamics of neuron-derived CGRP in vivo, providing an experimental basis in vitro for deciphering the spatiotemporal regulatory role of CGRP in bone microenvironment remodeling.

H&E staining results indicate that these materials exhibit good in vivo biocompatibility, as the tissue structures of major organs in rats from the H2G5 and H2G5@CGRP groups remained intact, with no obvious toxic damage observed (Figure 5A). At 4 weeks, a slight amount of new bone formed in the skull defect area from the H2G5 group, while the H2G5@CGRP group exhibited noticeable new bone formation and a significant increase in trabecular bone. At 8 weeks, bone volume in the defect area of the H2G5 group had increased, but most of the area still exhibited low-density shadows. In contrast, the H2G5@CGRP group displayed extensive mature bone tissue filling the defect, with dense and continuous trabecular bone and well-restored cortical bone structure (Fig. 5B). Quantitative analysis results demonstrated that BV/TV, Tb.N, and Tb.Th in the H2G5@CGRP group were substantially increased compared with the H2G5 group at both Week 4 and Week 8 (Fig. 5C, $P<0.05$). This suggests that, within the microenvironment of a localized bone defect, the continued release of CGRP promotes the reconstruction of trabecular microstructure, increases trabecular number and thickness, and enhances the bone volume fraction, thereby significantly enhancing bone regeneration and bone mass recovery.

Histological evaluation was performed to assess CGRP-mediated bone regeneration. H&E staining showed that the H2G5 group formed substantial loose connective tissue in the central defect area, whereas the H2G5@CGRP group exhibited dense collagen fibers connecting the original and

newly formed bone tissues at the defect margins (Fig. 6A). Masson staining results showed that at 4 weeks, the H2G5 group displayed a small amount of blue collagen fiber deposition with sparse newly formed bone, while the H2G5@CGRP group showed abundant blue collagen matrix accompanied by early trabecular-like structure formation in the defect area. At 8 weeks, the H2G5 group exhibited further increased collagen deposition but incomplete bone repair, whereas the H2G5@CGRP group showed extensive mature bone tissue filling the defect, with Masson staining revealing dense deep-blue collagen, abundant trabecular bone, and well-formed bone marrow cavities, demonstrating the most pronounced osteogenic repair effect (Fig. 6B).

To further elucidate the mechanism of CGRP-mediated bone regeneration, a systematic IHC analysis was performed on osteogenic marker proteins, including BMP4, OCN, TGF-β, and Smad2/3. Brown immunoreactive deposits were uniformly distributed throughout the microenvironment of the bone defect. The results demonstrated that the H2G5@CGRP hydrogel exhibits potent osteogenic potential in vivo, with expression levels of TGF-β, Smad2/3, OCN, and BMP4 were markedly higher than those in the H2G5 group at 4 and 8 weeks (Fig. 7A-H, $P<0.05$). These spatiotemporal dynamic changes imply that CGRP may accelerate bone regeneration and repair of cranial defects by activating the TGF-β/Smad2/3 axis.

In summary, the CGRP @ H2G5 hydrogel effectively promotes new bone formation and collagen deposition at the cranial defect site through sustained delivery of CGRP to the defect site, and upregulates the expression of osteogenic markers OCN, BMP4, TGF-β, and Smad2/3, accompanied by the activation of the TGF-β/Smad2/3 signaling pathway.

4. Discussion

The process of bone regeneration is finely regulated by the nervous system. Bone tissue is not merely a passive recipient of conventional hormonal regulation, but is continuously modulated by both the central and peripheral nervous systems[6,34]. Sensory nerve fibers distributed on the periosteum and trabecular bone surfaces translate neural signals into chemical signals recognizable by bone tissue through the release of various bioactive molecules, thereby dynamically responding to changes in the local microenvironment[35]. This study, centered on the question of "how transient sensory neuropeptide stimulation is converted by BMSCs into an osteogenic differentiation response," constructed a continuous chain of evidence encompassing transcriptomic screening, in vitro functional validation, signaling pathway blockade, and in vivo bone regeneration evaluation.

As a classic neuropeptide released by sensory neurons, CGRP has been closely associated with bone formation, fracture healing, and tissue repair[36]. We conducted a series of in vitro functional experiments to evaluate the effects of CGRP on the biological behavior of BMSCs. Results from CCK-8 and Transwell assays demonstrated that CGRP effectively promotes the proliferation and chemotactic migration of BMSCs. ALP and ARS staining confirmed that CGRP promotes early osteogenic differentiation and terminal mineralization of BMSCs. Based on the aforementioned phenotypic evidence, we conclude that CGRP, as a key mediator of the neuro-osseous axis, can directly target BMSCs to drive the bone regeneration process.

To further dissect the molecular basis underlying CGRP-induced functional changes in BMSCs, we performed RNA-seq analysis to profile the transcriptomic response following CGRP treatment. The results revealed that 275 DEGs were significantly altered after CGRP intervention, suggesting that CGRP induced a relatively focused rather than widespread and indiscriminate transcriptional response. GO analysis indicates that these DEGs are primarily associated with a range of biological processes, which include cell adhesion, migration, proliferation regulation, inflammatory responses, and extracellular matrix remodeling. These processes are closely related to BMSC recruitment, proliferation, and osteogenic differentiation during bone defect repair. GSEA results demonstrated enrichment of gene sets related to DNA replication and chromosome segregation, consistent with the pro-proliferative phenotype detected by CCK-8 assays. Thus, CGRP may first enhance the cellular substrate available for participation in injury repair by promoting BMSC proliferation and migration, and subsequently further facilitate the initiation of osteogenic molecular programs in an osteogenic inductive environment.

KEGG analysis suggests that the TGF-β signaling pathway may be involved with the CGRP-induced response in BMSCs. Therefore, in this study, we used immunofluorescence, qRT -PCR, and Western blotting. CGRP treatment increased TGF-β expression and Smad2/3 nuclear translocation in BMSCs, as well as the mRNA and protein expression of osteogenic factors (ALP, RUNX2, and BMP4). The TGF-β family primarily contributes to the maintenance of bone homeostasis by regulating the recruitment, migration, proliferation, and differentiation of MSCs[37] through the classic downstream Smad2/3 signaling pathway, which mediates their nuclear translocation and regulates the expression of osteogenic genes[38,39].

More importantly, TGF-β signaling inhibition experiments further reinforced the causal nature

of the above mechanistic chain. Simply observing enhanced TGF-β/Smad2/3 signaling after CGRP treatment indicates only a correlative relationship. However, our study revealed that, following the addition of a TGF-β inhibitor, CGRP-induced migration of BMSCs, ALP differentiation, calcium nodule formation, and osteogenic factor expression were all significantly reduced. This suggests that TGF-β/Smad2/3 signaling is not only an accompanying phenomenon following CGRP treatment but also plays a crucial functional role in CGRP-induced osteogenic differentiation of BMSCs. These findings support that CGRP stimulation induces a TGF-β/Smad2/3-related signaling response in BMSCs, accompanied by enhanced osteogenic transcriptional programming.

In addition to validating this mechanism in vitro, this study also used a rat cranial defect model to evaluate the effects of CGRP@H2G5 hydrogel delivery on bone regeneration. Given that CGRP degrades rapidly in vivo, a simple local injection alone is insufficient to maintain an effective duration of action in the site of the bone defect. Therefore, employing the hydrogel as a local delivery system helps prolong the retention and action window of CGRP in the defect region, better mimicking the sustained release of CGRP by sensory nerves. Notably, as the implantation time extended from 4 to 8 weeks, the H2G5@CGRP group consistently maintained a significant advantage over the H2G5 group in the three core parameters-BV/TV, Tb.N, and Tb.Th. This not only confirms the sustained osteogenic effect of this system, but also indicates that the incorporation of CGRP effectively bridges osteoconduction and osteoinduction, thereby promoting the transition of newly formed bone tissue from early loose woven bone to a more compact and robust lamellar bone structure. Histological staining and IHC results indicate that local delivery of CGRP accelerates collagen matrix deposition and bone formation in bone defect sites, promotes bone maturation and the expression of osteogenesis-related molecules (OCN, BMP4), and that these in vivo bone regeneration effects may be associated with the activation of the TGF-β/Smad2/3 signaling pathway.

Admittedly, this study has certain limitations. A notable characteristic of most neuropeptides is that they are typically released by neurons via dense core vesicles at synapses and bind to G protein-coupled receptors with seven transmembrane domains[40,41]. According to current theories, CGRP binds to the calcitonin receptor-like receptor/receptor activity-modulating protein 1 (CALCRL/RAMP1) complex, activates Ca^{2+} channels, and triggers Ca^{2+} influx, thereby converting neural signals into intracellular signaling[42]. Although this study has clarified the role of the

CGRP/TGF-β/Smad2/3 axis in osteogenic differentiation, the early signaling events—specifically, how CGRP initiates signaling upon receptor binding and progressively leads to Smad2/3 phosphorylation—remain unclear. Further research is needed to elucidate this upstream signaling cascade in order to fully uncover the molecular regulatory pathways governing the transition from neuropeptide sensing to osteogenic differentiation. In addition, the sample size used in the in vivo experiments in this study was set rather conservatively; although statistically significant differences were detected, the reliability of these results still needs to be verified through studies with larger sample sizes. Finally, this study provides in vivo evidence supporting the involvement of the TGF-β/Smad2/3 pathway in CGRP-mediated bone regeneration. To rigorously establish its necessity, future studies will utilize specific conditional knockout mice to determine whether this pathway is essential for CGRP-mediated bone regeneration in vivo.

Overall, based on existing data and classical receptor theory, we propose a “neuro-osseous axis” cascade activation hypothesis to elucidate the molecular mechanism by which the neuropeptide CGRP mediates osteogenic differentiation. This hypothesis posits that CGRP interacts with BMSCs, triggering a robust intracellular signaling cascade that activates downstream pathways for osteogenic differentiation in BMSCs. At the molecular level, CGRP first activates the expression of TGF-β and TGF-βR, thereby initiating a Smad2/3 phosphorylation cascade. Once the activated Smad2/3 complex is translocated to the cell nucleus, its specific recognition and binding to the promoter regions of target genes ultimately lead to the transcriptional activation of RUNX2 and BMP4—both of which synergistically promote osteogenic differentiation. In this way, the transient chemical signals detected by membrane receptors are translated into a sustained and specific osteogenic transcriptional program within the cell nucleus (Fig. 8).

The significance of this study lies in linking the osteogenic action of the sensory neuropeptide CGRP with the osteogenic signaling response within BMSCs, proposing a relatively comprehensive mechanistic framework for the translation of sensory neuropeptide signals into BMSC osteogenic programs and subsequent bone regeneration. Unlike merely demonstrating that CGRP possesses osteogenic effects, this study first screened out the TGF-β signaling pathway via RNA-seq, then confirmed its functional role in CGRP-induced osteogenesis through in vitro signaling validation and blockade experiments, and finally verified the in vivo bone regenerative effects through local CGRP delivery. Therefore, this study provides new experimental evidence for understanding how

transient neuropeptide stimulation is converted by BMSCs into an osteogenic differentiation response.

5. Conclusion

In summary, this study constructed a continuous chain of evidence spanning from *in vitro* transcriptomic screening and targeted signaling pathway inhibition to *in vivo* biomimetic delivery and bone regeneration evaluation. RNA-seq analysis revealed that CGRP intervention in BMSCs significantly enriched the TGF-β signaling pathway. In vitro experiments demonstrated that CGRP was correlated with the cascade activation and nuclear translocation of TGF-β/Smad2/3 signaling, effectively promoting BMSC proliferation, migration, and osteogenic differentiation, while blockade of TGF-β signaling attenuated its pro-osteogenic effects, thereby supporting the involvement of TGF-β/Smad2/3 in the osteogenic response induced by CGRP at the functional level in vitro. More importantly, in vivo application of the H2G5-CGRP photocurable hydrogel, which enables local sustained release of CGRP, appeared to initiate a sustained osteogenic program by effectively prolonging the duration of neuropeptide action, significantly up-regulating osteogenic protein expression, and accelerating new bone formation in calvarial defects. This in vivo process is accompanied by the activation of the TGF-β/Smad2/3 signaling pathway, providing correlative in vivo evidence supporting the involvement of this pathway in the bone regeneration mediated by CGRP.

Author Contributions

Xi Wang: Writing-original draft, Writing-review & editing, Methodology, Visualization, Funding acquisition. **Qiyu Jia:** Writing-review & editing, Methodology, Formal analysis, Funding acquisition. **Maihemuti Yakufu:** Investigation, Funding acquisition. **Jinyong Huang:** Visualization, Resources. **Junru Liao:** Data Curation, Methodology. **Jun Zhang:** Methodology. **Meng Zhao:** Software-validation. **Jingcheng Hu:** Formal analysis. **Yanbin Zhu:** Writing-review & editing, Methodology. **Chuang Ma:** Supervision, Conceptualization, Funding acquisition, Project administration.

Declaration of competing interest

The authors declare that they have no competing interests.

Data availability

The RNA-seq data generated in this study have been deposited in the NCBI GEO under accession number GSE352508.

Declaration of AI use

In the process of writing this paper, the DeepSeek generative artificial intelligence tool is used, which is mainly used for language polishing, grammar checking and readability optimization of manuscripts. After using this tool, the author verifies the generated content one by one and makes necessary modifications, and assumes full responsibility for the integrity, accuracy and academic standardization of the paper.

Funding

This study was funded by the National Natural Science Foundation of China (82260425 and 82604707), the Xinjiang Uygur Autonomous Region Health Science and Technology Plan Project (2025001CGZHYDXM650030090), the Xinjiang Uygur Autonomous Region Key Research and Development Special Project (2022B03013-6), the Postgraduate Research Innovation Project of Xinjiang Uygur Autonomous Region (XJ2026G146), the Research and Innovation Team Project of Xinjiang Medical University (XYD2024C12), the Tianshan Innovation Team Program (2025D14019), and the Research and Innovation Team Project of the Sixth Affiliated Hospital of Xinjiang Medical University (LFYKYZXJJ2024001).

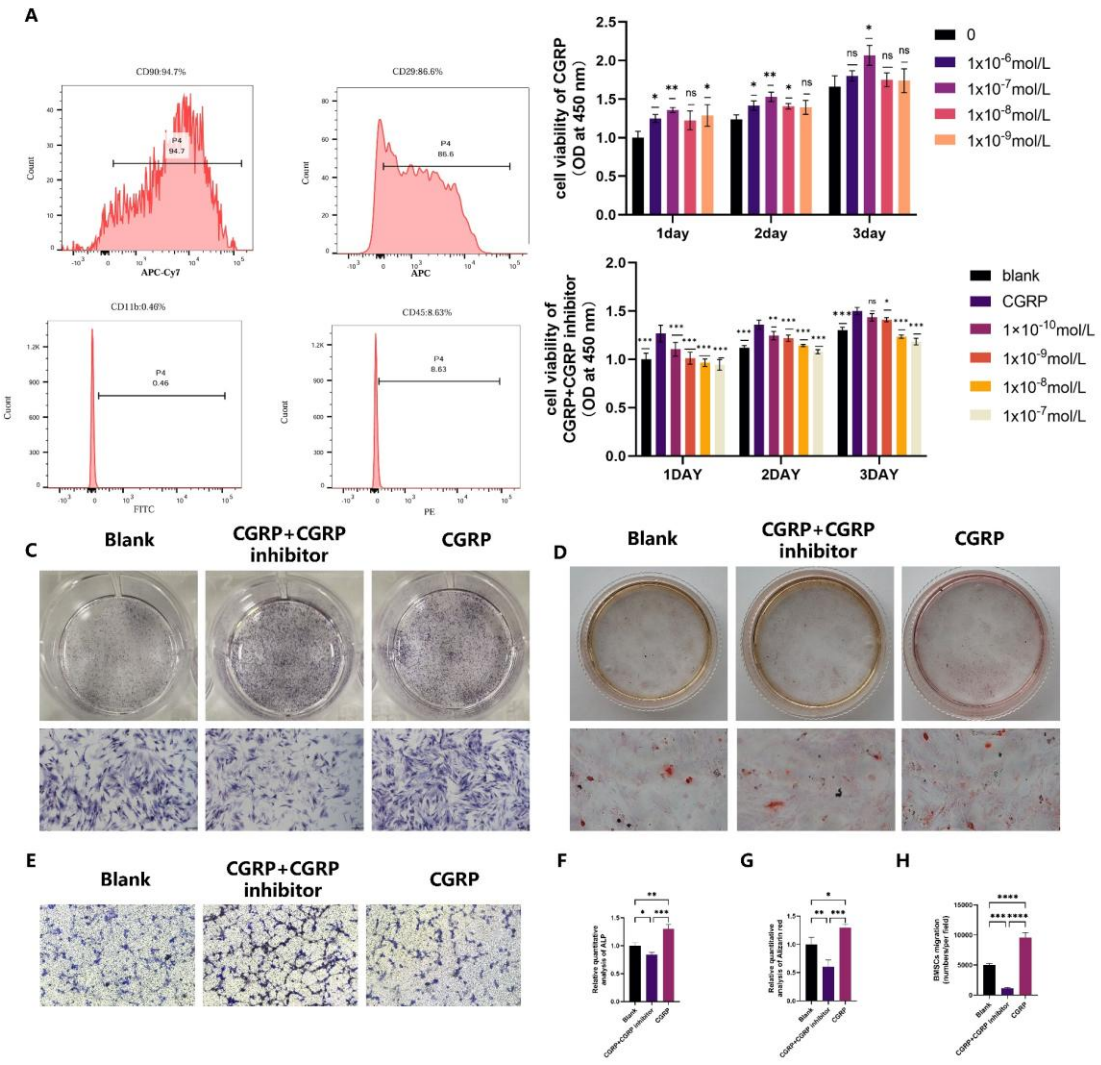


Fig. 1. CGRP promotes BMSCs proliferation, migration, and osteogenic differentiation.

(A) Flow cytometric identification of BMSCs purity. (B) CCK-8 to determine the effects of CGRP alone and CGRP combined with its receptor antagonist on the proliferation of BMSCs. (C) ALP staining evaluating early osteogenic differentiation capacity of BMSCs following CGRP treatment. (D) ARS staining assessing late osteogenic mineralization capacity of BMSCs after CGRP treatment. (E) Transwell staining evaluating the migratory capacity of BMSCs upon CGRP stimulation. Quantitative analysis results of ALP staining (F), ARS staining(G), and Transwell assay (H). (Mean±SD, n=3. $^{*}P<0.05$, $^{**}P<0.01$, $^{***}P<0.001$, $^{****}P<0.0001$ and ns, not significant.)

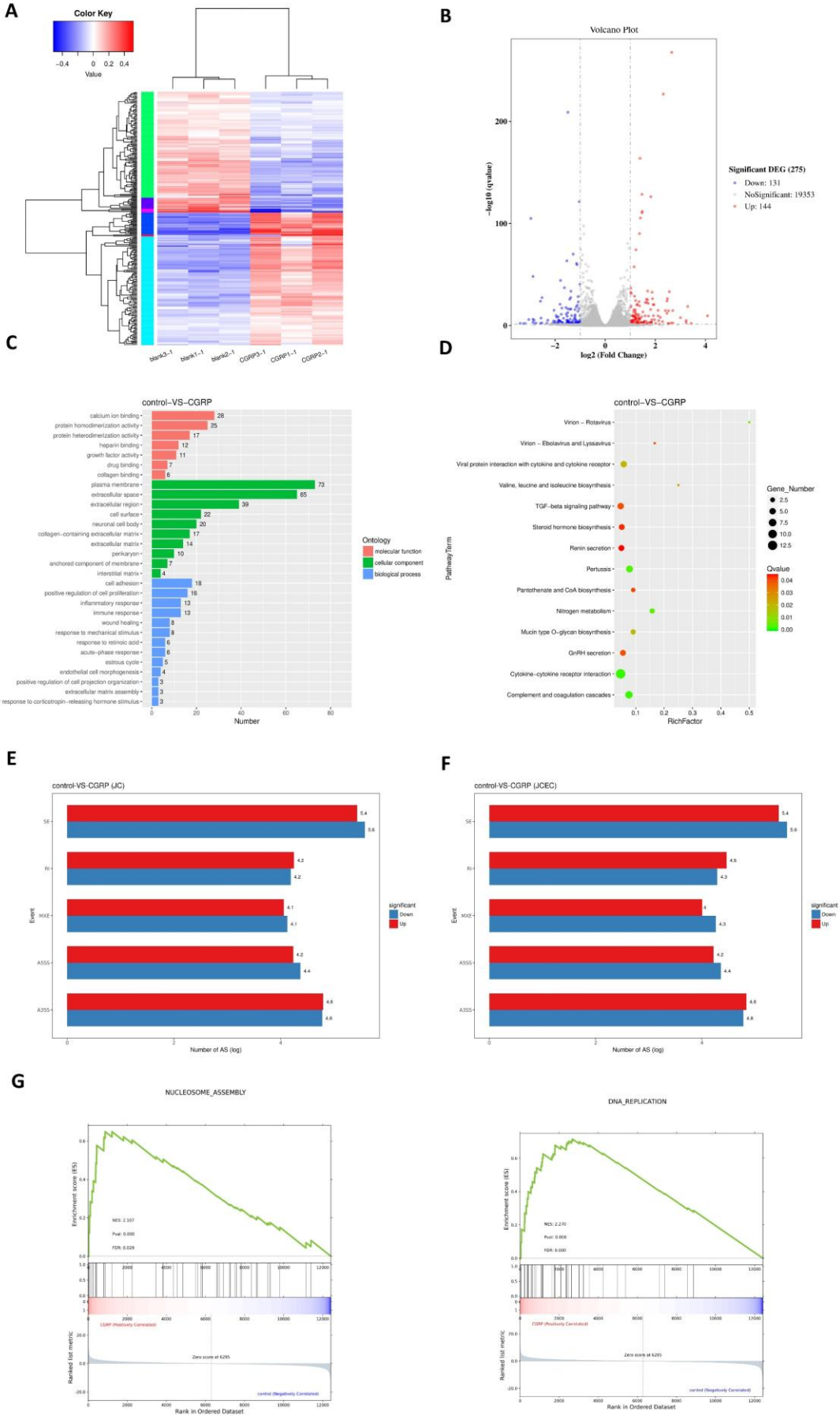

A
Color Key
Value
blank3_1
blank1_1
blank2_1
CGRP3_1
CGRP1_1
CGRP2_1
B
Volcano Plot
−log10 (qvalue)
log2 (Fold Change)
Significant DEG (275)
Down: 131
NoSignificant: 19353
Up: 144
C
control−VS−CGRP
GO Term
Number
Ontology
molecular function
cellular component
biological process
calcium ion binding
protein homodimerization activity
protein heterodimerization activity
heparin binding
growth factor activity
drug binding
collagen binding
plasma membrane
extracellular space
extracellular region
cell surface
neuronal cell body
collagen−containing extracellular matrix
extracellular matrix
perikaryon
anchored component of membrane
interstitial matrix
cell adhesion
positive regulation of cell proliferation
inflammatory response
immune response
wound healing
response to mechanical stimulus
response to retinoic acid
acute−phase response
estrous cycle
endothelial cell morphogenesis
positive regulation of cell projection organization
extracellular matrix assembly
cellular response to corticotropin−releasing hormone stimulus
D
control−VS−CGRP
Pathway Term
RichFactor
Gene_Number
Qvalue
Virion − Rotavirus
Virion − Ebolavirus and Lyssavirus
Viral protein interaction with cytokine and cytokine receptor
Valine, leucine and isoleucine biosynthesis
TGF−beta signaling pathway
Steroid hormone biosynthesis
Renin secretion
Pertussis
Pantothenate and CoA biosynthesis
Nitrogen metabolism
Mucin type O−glycan biosynthesis
GnRH secretion
Cytokine−cytokine receptor interaction
Complement and coagulation cascades
E
control-VS-CGRP (JC)
Event
Number of AS (log)
significant
Down
Up
SE
RI
MXE
A5SS
A3SS
F
control-VS-CGRP (JCEC)
Event
Number of AS (log)
significant
Down
Up
SE
RI
MXE
A5SS
A3SS
G
NUCLEOSOME_ASSEMBLY
DNA_REPLICATION
Enrichment score (ES)
Ranked list metric
Rank in Ordered Dataset
Zero score at 6295

Fig. 2. Transcriptomic profiling of BMSCs regulated by CGRP.

(A) Hierarchical clustering analysis of Control vs CGRP groups (Red indicates genes upregulated in BMSCs by CGRP; blue indicates genes downregulated in BMSCs by CGRP) (B) Volcano plot of Control vs CGRP groups. (C) GO analysis. (D) KEGG analysis. (E) Alternative splicing analysis (JC mode) of Control vs CGRP groups. (F) Alternative splicing analysis (JCEC mode) of Control vs CGRP groups. (G) GSEA analysis.

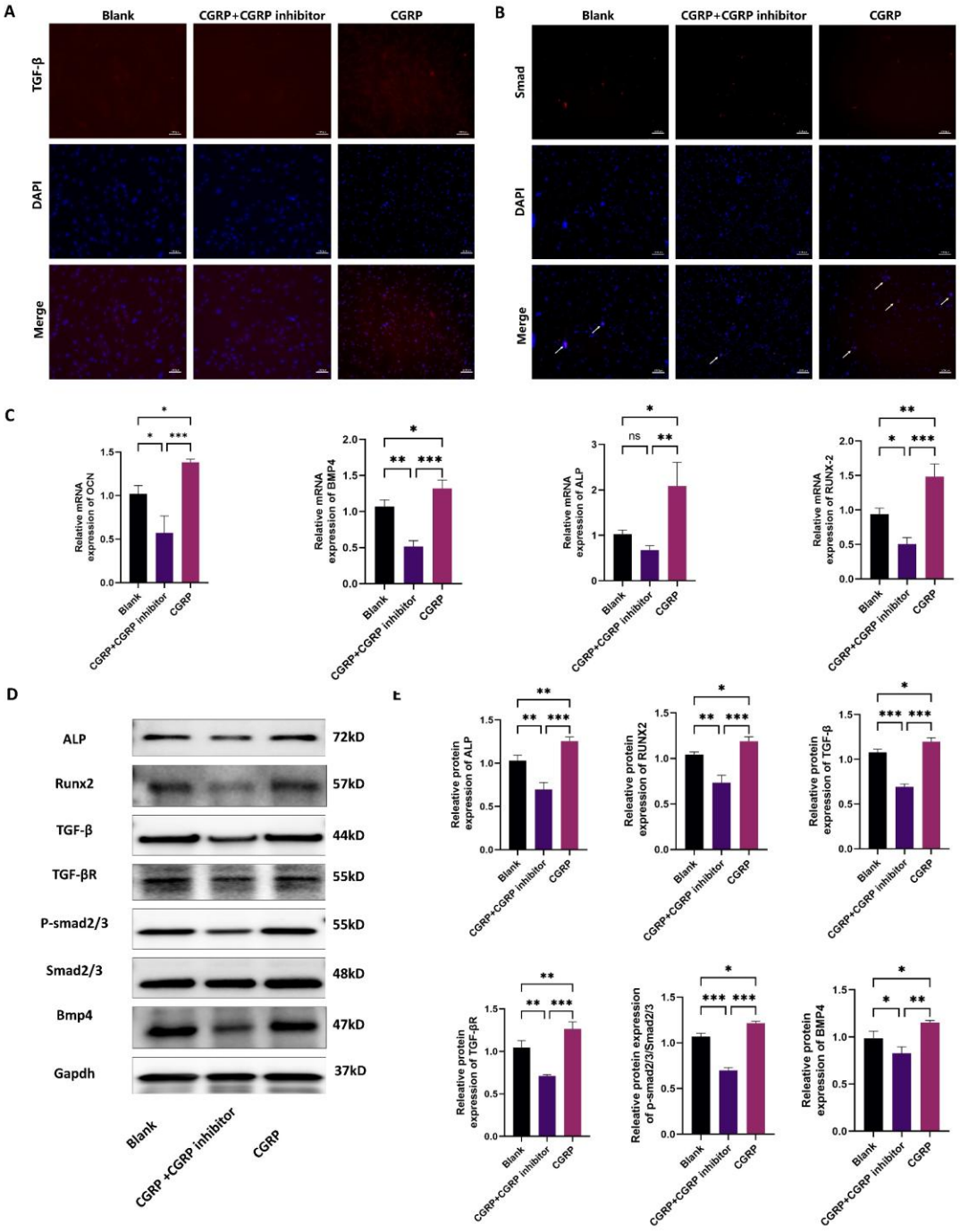


Fig. 3. CGRP promotes osteogenic differentiation through the TGF-β/Smad2/3 pathway.

(A-B) Immunofluorescence staining showing the subcellular localization of TGF-β (A) and Smad2/3 (B); (C) qRT-PCR of mRNA levels of osteogenesis-related genes (e.g., OCN, BMP4, Runx2, ALP); (D-E) Western blot of the expression of osteogenesis-related proteins (D) and quantitative analysis of their gray-scale intensity (E). (Mean ± SD, n=3. $^{*}P<0.05$, $^{**}P<0.01$, $^{***}P<0.001$, $^{****}P<0.0001$ and ns, not significant.)

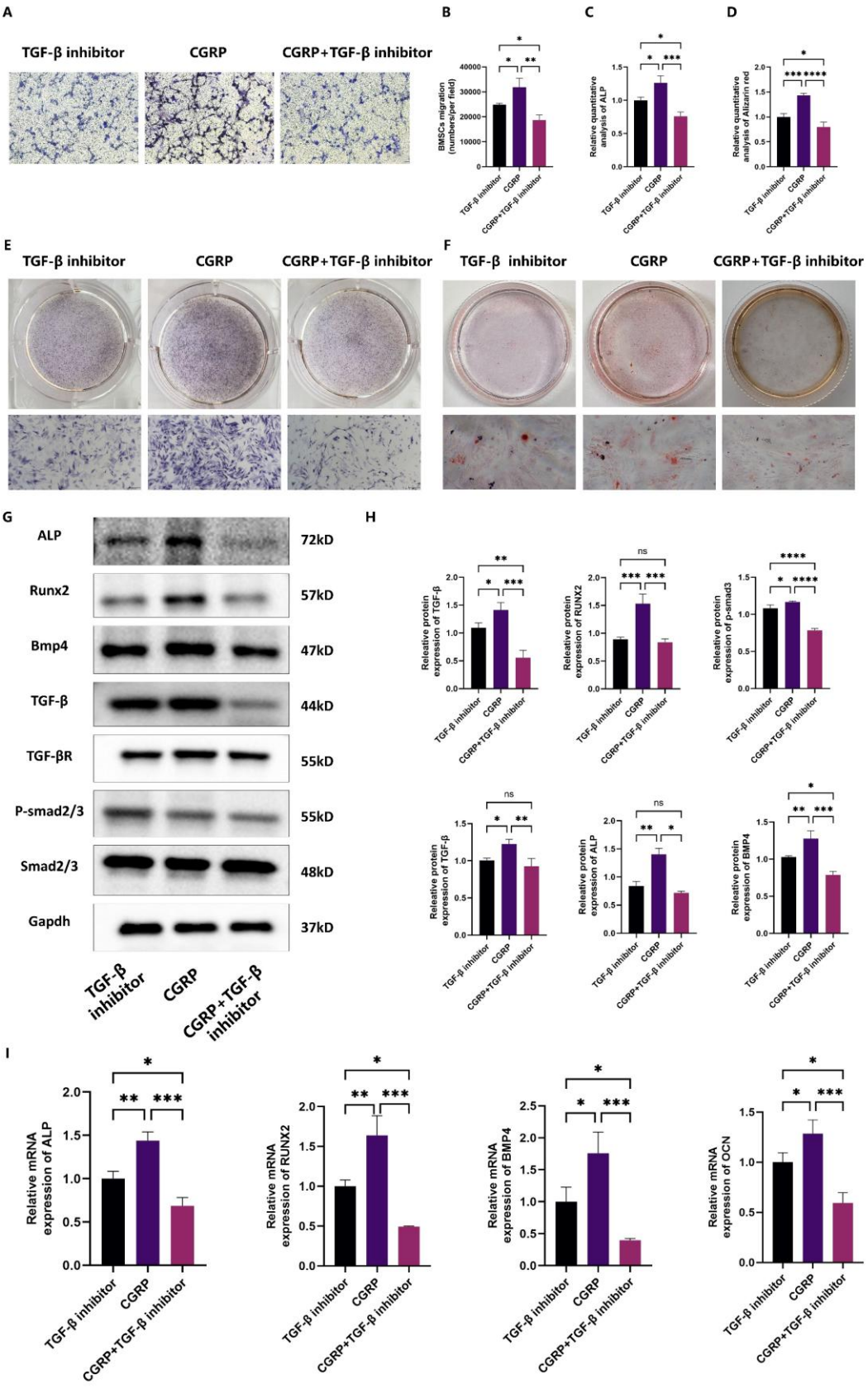


Fig. 4. Inhibition of TGF-β significantly attenuates CGRP-mediated osteogenic differentiation of BMSCs.

(A-B) Transwell assay(A) and quantitative analysis(B); ALP staining assay (E) and its quantitative analysis (C); ARS staining (F) and its quantitative analysis (D); (G-H) Western blot (G) and quantitative analysis (H); (I) qRT-PCR. (Mean±SD, n=3. $^{*}P<0.05$, $^{**}P<0.01$, $^{***}P<0.001$, $^{****}P<0.0001$ and ns, not significant.)

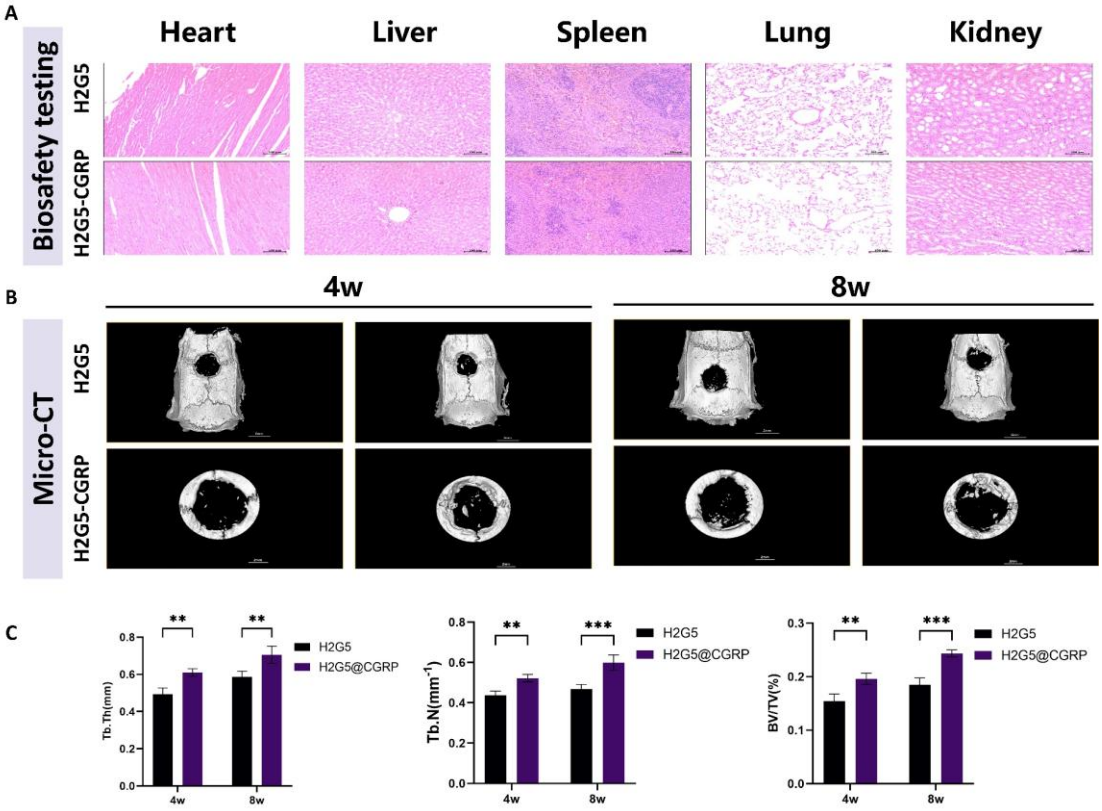


Fig. 5. The H2G5@CGRP hydrogel can promote in situ bone regeneration at cranial defects in rats.

(A) H&E staining evaluating the biocompatibility of H2G5@CGRP hydrogel. (B) Micro-CT. (C) Quantitative analysis of Micro-CT. (At each time point, each group consisted of 3 animals as independent biological replicates. Mean±SD, $^{*}P<0.05$, $^{**}P<0.01$, $^{***}P<0.001$, $^{****}P<0.0001$ and ns, not significant.)

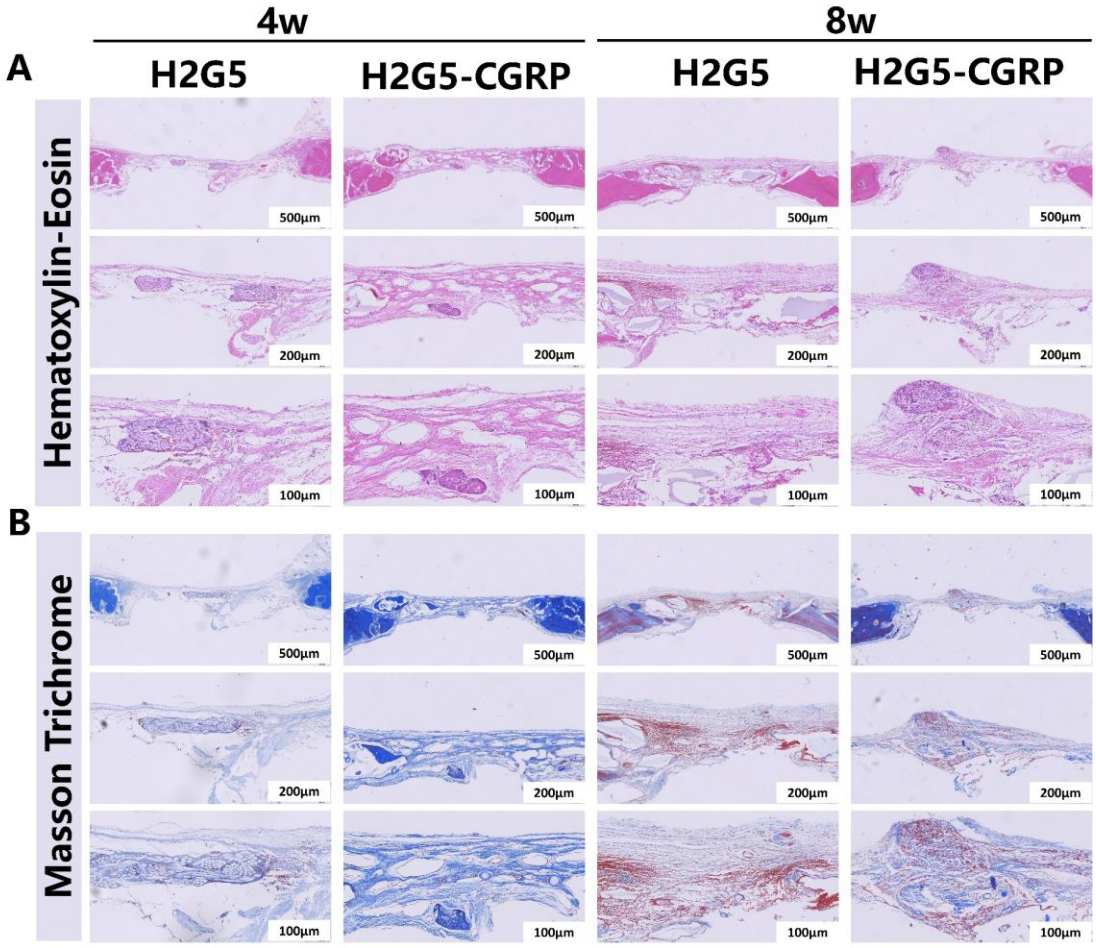
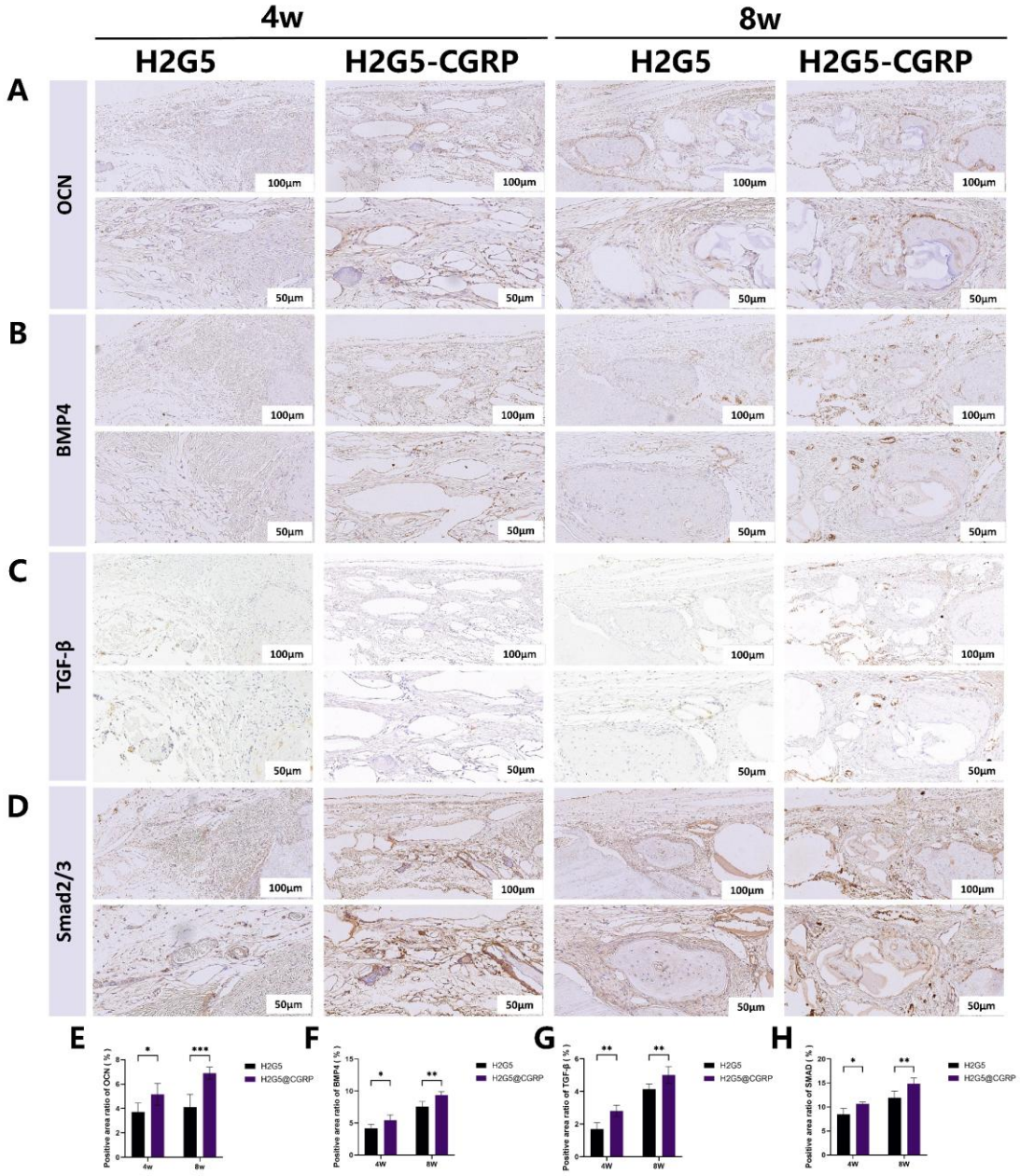


Fig. 6. Histological Evaluation of H2G5@CGRP Hydrogel-Mediated Bone Regeneration in Rat Skull Defects

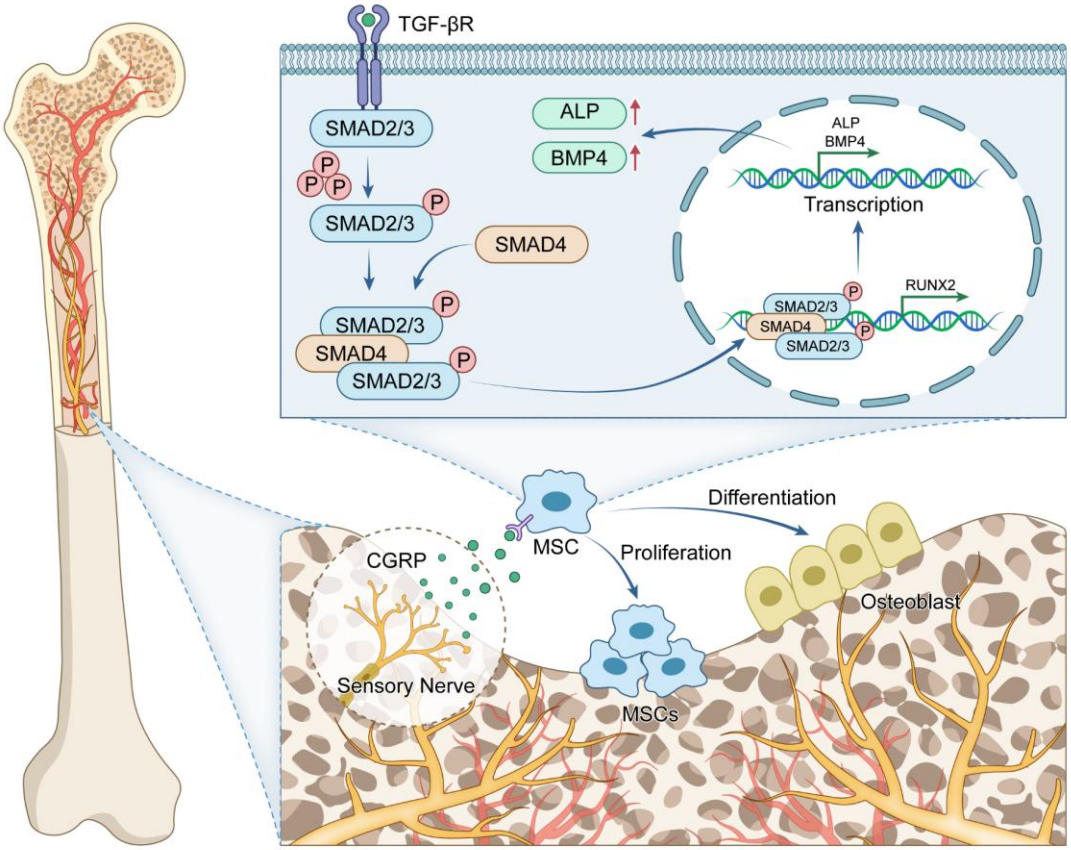
(A) H&E staining of cranial defects in rats from each group at 4 and 8 weeks post-surgery; (B) Masson's staining of cranial defects in rats from each group at 4 and 8 weeks post-surgery (image scales: 100 μm, 200 μm, and 500 μm)



675

676 **Fig. 7. H2G5@CGRP hydrogels promote bone regeneration in rat calvarial defects**
677 **accompanied by TGF-β/Smad2/3 pathway activation**

678 (A-D) IHC staining of OCN, BMP4, TGF-β, and Smad2/3 in the defect areas. (E-H) Quantitative
679 analysis of IHC staining. (At each time point, each group consisted of 3 animals as independent
680 biological replicates. Mean±SD, $^{*}P<0.05$, $^{**}P<0.01$, $^{***}P<0.001$, $^{****}P<0.0001$ and ns, not
681 significant.)



682

683 **Fig. 8. The CGRP-TGF-β/Smad2/3 axis detects signals from sensory neuropeptides and drives**

684 **the osteogenic program, promoting bone regeneration**

685 **Table 1. Primer Sequence**

Gene	primer sequences（5'-3'）
Runx2	F: CCTTCAAGGTTGTAGCCCTC
	R: GGAGTAGTTCTCATCATTCCCG
ALP	F: TCATTCCCACGTTTTCACATTC
	R: GTTGTTGTGAGCGTAATCTACC
OCN	F: CAAGCAGGAGGGCAATAAGGTAGTG
	R: CGGTCTTCAAGCCATACTGGTCTG
BMP4	F: GAACATCCCAGGGACCAGTG
	R: ATCCTGACATGTTGGCCCTG
Gapdh	F: GGCAAATTCAACGGCACAGTCAAG
	R: TCGCTCCTGGAAGATGGTGATGG

686

References

1 Koushik, T. M., Miller, C. M. & Antunes, E. Bone Tissue Engineering Scaffolds: Function of Multi-Material Hierarchically Structured Scaffolds. *Adv Healthc Mater* **12**, e2202766, doi:10.1002/adhm.202202766 (2023).

2 Dec, P., Modrzejewski, A. & Pawlik, A. Existing and Novel Biomaterials for Bone Tissue Engineering. *Int J Mol Sci* **24**, doi:10.3390/ijms24010529 (2022).

3 Wan, Q. Q. *et al.* Crosstalk between Bone and Nerves within Bone. *Adv Sci (Weinh)* **8**, 2003390, doi:10.1002/advs.202003390 (2021).

4 Qin, Q. *et al.* Neurovascular coupling in bone regeneration. *Exp Mol Med* **54**, 1844-1849, doi:10.1038/s12276-022-00899-6 (2022).

5 Sun, W. *et al.* Neuro-bone tissue engineering: emerging mechanisms, potential strategies, and current challenges. *Bone Res* **11**, 65, doi:10.1038/s41413-023-00302-8 (2023).

6 Lv, X., Gao, F. & Cao, X. Skeletal interoception in bone homeostasis and pain. *Cell Metab* **34**, 1914-1931, doi:10.1016/j.cmet.2022.09.025 (2022).

7 Chen, H. *et al.* Prostaglandin E2 mediates sensory nerve regulation of bone homeostasis. *Nat Commun* **10**, 181, doi:10.1038/s41467-018-08097-7 (2019).

8 Mi, J. *et al.* Implantable Electrical Stimulation at Dorsal Root Ganglions Accelerates Osteoporotic Fracture Healing via Calcitonin Gene-Related Peptide. *Adv Sci (Weinh)* **9**, e2103005, doi:10.1002/advs.202103005 (2022).

9 Chen, Y., Guo, B., Ma, G. & Cao, H. Sensory nerve regulation of bone homeostasis: Emerging therapeutic opportunities for bone-related diseases. *Ageing Res Rev* **99**, 102372, doi:10.1016/j.arr.2024.102372 (2024).

10 Appelt, J. *et al.* The neuropeptide calcitonin gene-related peptide alpha is essential for bone healing. *EBioMedicine* **59**, 102970, doi:10.1016/j.ebiom.2020.102970 (2020).

11 Li, Z. *et al.* Fracture repair requires TrkA signaling by skeletal sensory nerves. *J Clin Invest* **129**, 5137-5150, doi:10.1172/jci128428 (2019).

12 Zhang, Z. *et al.* Engineered Sensory Nerve Guides Self-Adaptive Bone Healing via NGF-TrkA Signaling Pathway. *Adv Sci (Weinh)* **10**, e2206155, doi:10.1002/advs.202206155 (2023).

13 Russo, A. F. & Hay, D. L. CGRP physiology, pharmacology, and therapeutic targets: migraine and beyond. *Physiol Rev* **103**, 1565-1644, doi:10.1152/physrev.00059.2021 (2023).

14 Zhang, Y. *et al.* Implant-derived magnesium induces local neuronal production of CGRP to improve bone-fracture healing in rats. *Nat Med* **22**, 1160-1169, doi:10.1038/nm.4162 (2016).

15 Crane, J. L. & Cao, X. Bone marrow mesenchymal stem cells and TGF-β signaling in bone remodeling. *J Clin Invest* **124**, 466-472, doi:10.1172/jci70050 (2014).

16 Grafe, I. *et al.* TGF-β Family Signaling in Mesenchymal Differentiation. *Cold Spring Harb Perspect Biol* **10**, doi:10.1101/cshperspect.a022202 (2018).

17 Wu, M., Wu, S., Chen, W. & Li, Y. P. The roles and regulatory mechanisms of TGF-β and BMP signaling in bone and cartilage development, homeostasis and disease. *Cell Res* **34**, 101-123, doi:10.1038/s41422-023-00918-9 (2024).

18 Miyazono, K., Maeda, S. & Imamura, T. Coordinate regulation of cell growth and differentiation by TGF-beta superfamily and Runx proteins. *Oncogene* **23**, 4232-4237,

731 doi:10.1038/sj.onc.1207131 (2004).
732 19 Josephs, T. M. *et al.* Structure and dynamics of the CGRP receptor in apo and peptide-
733 bound forms. *Science* **372**, doi:10.1126/science.abf7258 (2021).
734 20 Russell, F. A., King, R., Smillie, S. J., Kodji, X. & Brain, S. D. Calcitonin gene-related peptide:
735 physiology and pathophysiology. *Physiol Rev* **94**, 1099-1142,
736 doi:10.1152/physrev.00034.2013 (2014).
737 21 Yakufu, M. *et al.* Injectable biomimetic hybrid nanofibers for targeting cartilage in early
738 osteoarthritis treatment. *Chemical Engineering Journal* **490**, 151790,
739 doi:org/10.1016/j.cej.2024.151790 (2024).
740 22 Jia, Q. *et al.* A pH-responsive nanocarrier delivered by carbine-crosslinked hydrogel paints
741 for smart immunomodulation in arthroscopic cartilage repair. *Chemical Engineering*
742 *Journal* **524**, doi:10.1016/j.cej.2025.169581 (2025).
743 23 Inman, G. J. *et al.* SB-431542 is a potent and specific inhibitor of transforming growth
744 factor-beta superfamily type I activin receptor-like kinase (ALK) receptors ALK4, ALK5, and
745 ALK7. *Mol Pharmacol* **62**, 65-74, doi:10.1124/mol.62.1.65 (2002).
746 24 Sun, K. *et al.* CGRP Regulates Nucleus Pulposus Cell Apoptosis and Inflammation via the
747 MAPK/NF-κB Signaling Pathways during Intervertebral Disc Degeneration. *Oxid Med Cell*
748 *Longev* **2021**, 2958584, doi:10.1155/2021/2958584 (2021).
749 25 Gai, T. *et al.* Sequential construction of vascularized and mineralized bone organoids using
750 engineered ECM-DNA-CPO-based bionic matrix for efficient bone regeneration. *Bioact*
751 *Mater* **49**, 362-377, doi:10.1016/j.bioactmat.2025.02.033 (2025).
752 26 Janmohammadi, M. *et al.* Evaluation of new bone formation in critical-sized rat calvarial
753 defect using 3D printed polycaprolactone/tragacanth gum-bioactive glass composite
754 scaffolds. *Int J Biol Macromol* **270**, 132361, doi:10.1016/j.ijbiomac.2024.132361 (2024).
755 27 Luo, J. *et al.* CGRP-Loaded Porous Microspheres Protect BMSCs for Alveolar Bone
756 Regeneration in the Periodontitis Microenvironment. *Adv Healthc Mater* **12**, e2301366,
757 doi:10.1002/adhm.202301366 (2023).
758 28 Kornblihtt, A. R. *et al.* Alternative splicing: a pivotal step between eukaryotic transcription
759 and translation. *Nat Rev Mol Cell Biol* **14**, 153-165, doi:10.1038/nrm3525 (2013).
760 29 Sherratt, D. J., Lau, I. F. & Barre, F. X. Chromosome segregation. *Curr Opin Microbiol* **4**,
761 653-659, doi:10.1016/s1369-5274(01)00265-x (2001).
762 30 Castellano Mdel, M., Boniotti, M. B., Caro, E., Schnittger, A. & Gutierrez, C. DNA replication
763 licensing affects cell proliferation or endoreplication in a cell type-specific manner. *Plant*
764 *Cell* **16**, 2380-2393, doi:10.1105/tpc.104.022400 (2004).
765 31 Xie, B. *et al.* Salidroside alleviates dexamethasone-induced inhibition of bone formation
766 via transforming growth factor-beta/Smad2/3 signaling pathway. *Phytother Res* **37**,
767 1938-1950, doi:10.1002/ptr.7711 (2023).
768 32 Asghar, M. S. *et al.* Dilation by CGRP of middle meningeal artery and reversal by
769 sumatriptan in normal volunteers. *Neurology* **75**, 1520-1526,
770 doi:10.1212/WNL.0b013e3181f9626a (2010).
771 33 Yakufu, M. *et al.* Carbene-mediated gelatin and hyaluronic acid hydrogel paints with ultra
772 adhesive ability for arthroscopic cartilage repair. *Int J Biol Macromol* **273**, 133122,
773 doi:10.1016/j.ijbiomac.2024.133122 (2024).
774 34 Li, J. *et al.* Emerging roles of nerve-bone axis in modulating skeletal system. *Med Res Rev*

44, 1867-1903, doi:10.1002/med.22031 (2024).
35 Elefteriou, F. Impact of the Autonomic Nervous System on the Skeleton. *Physiol Rev* **98**, 1083-1112, doi:10.1152/physrev.00014.2017 (2018).
36 Zhao, X., Wu, G., Zhang, J., Yu, Z. & Wang, J. Activation of CGRP receptor-mediated signaling promotes tendon-bone healing. *Sci Adv* **10**, eadg7380, doi:10.1126/sciadv.adg7380 (2024).
37 Jia, S. & Meng, A. TGFβ family signaling and development. *Development* **148**, doi:10.1242/dev.188490 (2021).
38 Mitra, S., Werner, C. & Dietz, D. M. Neuroadaptations and TGF-β signaling: emerging role in models of neuropsychiatric disorders. *Mol Psychiatry* **27**, 296-306, doi:10.1038/s41380-021-01186-y (2022).
39 Aashaq, S. *et al.* TGF-β signaling: A recap of SMAD-independent and SMAD-dependent pathways. *J Cell Physiol* **237**, 59-85, doi:10.1002/jcp.30529 (2022).
40 Nusbaum, M. P., Blitz, D. M. & Marder, E. Functional consequences of neuropeptide and small-molecule co-transmission. *Nature Reviews Neuroscience* **18**, 389-403, doi:10.1038/nrn.2017.56 (2017).
41 van den Pol, A. N. Neuropeptide transmission in brain circuits. *Neuron* **76**, 98-115, doi:10.1016/j.neuron.2012.09.014 (2012).
42 Walker, C. S., Conner, A. C., Poyner, D. R. & Hay, D. L. Regulation of signal transduction by calcitonin gene-related peptide receptors. *Trends Pharmacol Sci* **31**, 476-483, doi:10.1016/j.tips.2010.06.006 (2010).

Supplementary Files

This is a list of supplementary files associated with this preprint. Click to download.

- RawWesternblotimageshowninFigure4..jpg
- WBanalysis.xlsx
- RawWesternblotimageshowninFigure3..jpg
- TableS1.Totalnumberofdifferentiallyexpressedgenes..xlsx
- TableS2.DifferentialalternativesplicingA3SSeventsbetweentheControlandCGRPgroupsbasedonJCcounts..xlsx
- TableS3.DifferentialalternativesplicingA3SSeventsbetweentheControlandCGRPgroupsbasedonJCECcounts..xlsx
- TableS4.DifferentialalternativesplicingA5SSeventsbetweentheControlandCGRPgroupsbasedonJCcounts..xlsx
- TableS5.DifferentialalternativesplicingA5SSeventsbetweentheControlandCGRPgroupsbasedonJCECcounts..xlsx
- TableS6.DifferentialalternativesplicingMXEeventsbetweentheControlandCGRPgroupsbasedonJCcounts..xlsx
- TableS7.DifferentialalternativesplicingMXEeventsbetweentheControlandCGRPgroupsbasedonJCECcounts..xlsx
- TableS8.DifferentialalternativesplicingRIeventsbetweentheControlandCGRPgroupsbasedonJCcounts..xlsx
- TableS9.DifferentialalternativesplicingRIeventsbetweentheControlandCGRPgroupsbasedonJCECcounts..xlsx
- TableS10.DifferentialalternativesplicingSEeventsbetweentheControlandCGRPgroupsbasedonJCcounts..xlsx
- TableS11.DifferentialalternativesplicingSEeventsbetweentheControlandCGRPgroupsbasedonJCECcounts..xlsx
- SupplementaryMaterials.docx